

# Atmospheric reflection during an anomalous low-state of Hercules X-1

Martin Still<sup>1</sup>

*NASA/Goddard Space Flight Center, Code 662, Greenbelt, MD 20771*

*Physics and Astronomy, University of St Andrews, North Haugh, St Andrews, Fife KY16 9SS, UK*

Kieran O'Brien, Keith Horne

*Physics and Astronomy, University of St Andrews, North Haugh, St Andrews, Fife KY16 9SS, UK*

Bram Boroson, Lev G. Titarchuk, Kimberly Engle<sup>2</sup>

*NASA/Goddard Space Flight Center, Greenbelt, MD 20771*

Saeqa D. Vrtilek

*Harvard-Smithsonian Center for Astrophysics, 60 Garden Street, Cambridge, MA 02138*

Hannah Quaintrell

*Department of Physics, The Open University, Milton Keynes MK7 6AA, UK*

Hauke Fiedler

*Institut of Astronomy and Astrophysics, Ludwig-Maximilian University, D-81679 Munich, Germany*

## ABSTRACT

We present *RXTE* observations of the eclipsing X-ray binary Hercules X-1 conducted during an anomalous low state. Data reduction reveals a light curve over 2.7 orbital cycles remarkably similar to optical and UV light curves which are dominated by the companion star. Count rates are modulated close to the orbital period, attaining a maximum when the inner face of the companion star, irradiated by X-rays from the compact source, is most-visible. Cold reflection provides an acceptable fit to the energy spectrum. Employing binary geometry to scale the model and assuming companion star reflection, we are able to reconstruct the incident X-rays which are removed from our direct line-of-sight (presumably by the accretion disk). We find the flux of the hidden source to be identical to the observed flux of Her X-1 at the peak of its main-high state. Consequently, Her X-1 is emitting a reflected spectrum, largely uncontaminated by direct X-rays in the anomalous low-state. The spectral energy distribution, period, amplitude and phasing of the modulation are all consistent with a companion star origin. Since this source occurs in a well-understood binary environment, it provides an excellent case study for more sensitive experiments in the future.

*Subject headings:* binaries: close – binaries: eclipsing – pulsars: individual (Hercules X-1) – radiative transfer – stars: neutron – X-rays: stars

## 1. Introduction

Her X-1 (Tananbaum et al. 1972) is an eclipsing X-ray binary containing a pulsar of  $1.4 M_{\odot}$  and an A7 stellar companion of  $2.2 M_{\odot}$  (Middleditch & Nelson 1976; Reynolds et al. 1997). The system displays behaviour on four separate periods – the pulsar spin (1.24-s), the binary orbit (1.7-d), a super period of 35-d which results from a retrograde-precessing, warped accretion disk, and a beat between the precessional and orbital periods of 1.62-d. The warp phenomenon is poorly understood but its source is likely to be a combination of both tide- and radiation-driven precession (Papaloizou & Tarquem 1995; Pringle 1996).

The 35-d super-cycle results in two phases of strong X-ray activity per cycle (Giacconi et al. 1973; Scott & Leahy 1999). The main-high state has a rapid turn-on over  $\sim 90$ -m and decays over  $\sim 10$ -d. An off-state where flux remains at  $\sim 1$  percent of the main-high state level follows for the next  $\sim 10$ -d, succeeded by a second short-high state, lasting  $\sim 5$ -d, with flux peaking at  $\sim 30$  percent of maximum. A further off-state completes the cycle and extends over the next  $\sim 10$ -d. The accretion disk casts a shadow over the surface of the companion star which migrates across the star on the beat frequency. The super-cycle is consequently observed at UV and optical energies which are dominated by X-ray emission reprocessed in the stellar atmosphere (Gerend & Boynton 1976).

The 35-d clock has remained mostly coherent since its discovery. There have however been three occasions when the clock has missed several consecutive turn-ons, or main-high flux has been reduced (Parmar et al. 1985; Vrtilek et al. 1994; Parmar et al. 1999). The cause of these anomalous low-states is not clear, but probably result from changes in the state of the accretion disk, either through an increase in vertical scale height, or disruption to the disk warp. However the level of reprocessed UV and optical flux from the companion star during these states suggests that the intrinsic X-ray flux, and presumably the accretion rate, remains mostly unaffected by this event (Vrtilek et al. 1994; 2001). The high orbital inclination of the binary indicates that perhaps just a

small variation in the disk geometry will block direct X-rays from our line-of-sight, while the companion stars view remains largely unchanged over much of its surface area.

The latest anomalous low-state began during 1999 Feb (Parmar et al. 1999) and the on-states had not recovered four cycles later when the current observations were scheduled. These were part of a simultaneous multi-wavelength campaign on Her X-1 described by Vrtilek et al. (2001). Results from simultaneous Hubble Space Telescope orbits are detailed by Boroson et al. (2000) and Boroson et al. (2001), and an earlier epoch of short-high state visits with *RXTE* by Still et al. (2001).

The current *RXTE* data reveal many similarities between the X-ray light curve and its optical/UV counterparts, suggesting that much of the anomalous low state X-ray emission could be of companion star origin. We find that cold Compton reflection is a statistically acceptable model for the energy spectrum and a reflection surface the size and distance from the pulsar of the companion star gives a good prediction of the incident X-ray flux provided this is identical to the peak of the normal on-state intensity. The possible detection of a relatively clean reflection spectrum in a well-determined binary geometry, free of dominant direct X-rays, would be a valuable resource for investigators of reflecting atmospheres in the less well-determined environments of AGN and stellar black hole candidates (Lightman & White; White, Lightman and Zdziarski 1988).

## 2. Observations

*RXTE* pointed at Her X-1 intermittently between 1999 July 11–16 (MJD 51 370.83–51 375.37) accumulating 100-ksec of time-tagged events. Event reconstruction was performed using standard algorithms within *FTOOLS* v4.2. We analyze data from the Proportional Counter Array (PCA; Zhang et al. 1993) in which three of the five identical Xe Proportional Counting Units (PCUs) were operational with a combined effective area of  $3900 \text{ cm}^2$ . As well as the standard data formats, we employ two event analyzers in the GoodXenon event mode with 2-s readout – timestamps are resolved to  $1\text{-}\mu\text{s}$ , while employing the full 256 energy channels (2.2–119.0 keV during epoch 4). Response

---

<sup>1</sup>Universities Space Research Association

<sup>2</sup>SSAI, 5900 Princess Garden Parkway, Suite 300, Lanham MD 20706

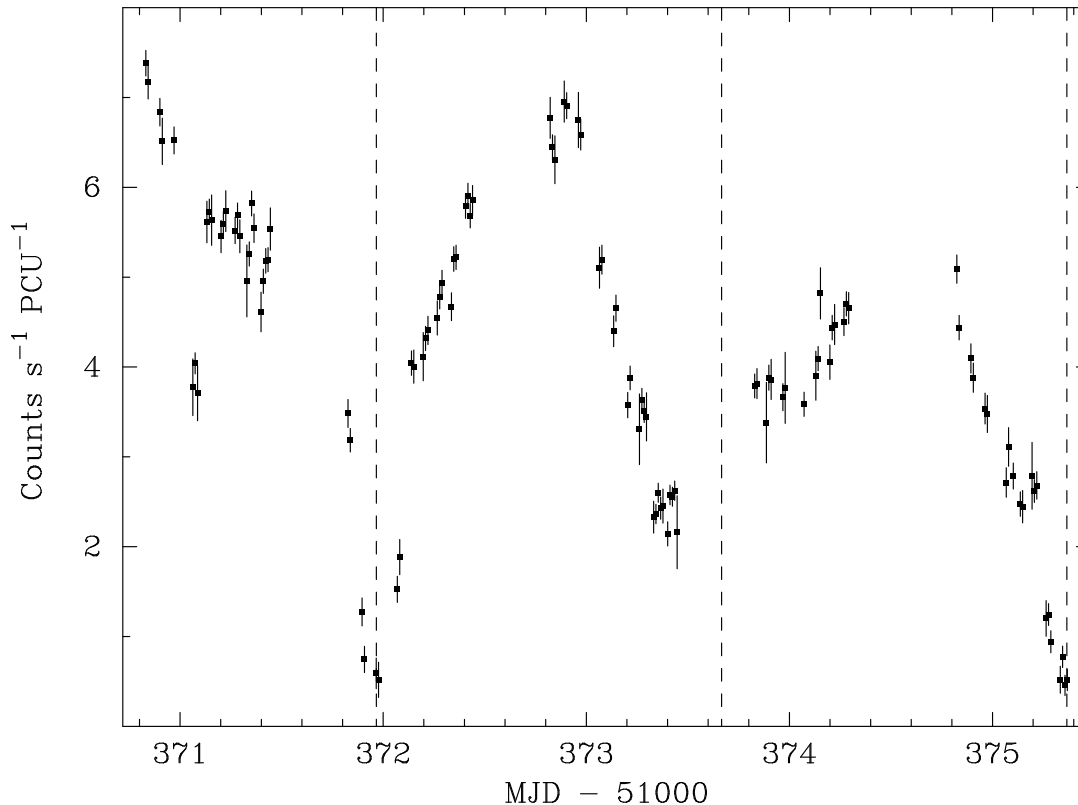


Fig. 1.— The 3–30 keV band light curve over the duration of the observations. The vertical dashed lines correspond to superior conjunction of the neutron star, according to the orbital ephemeris of Deeter et al. (1991).

matrices from 1999 Mar 30 were obtained from the HEASARC archive<sup>3</sup>. Background estimates are derived from the Very Large Event model<sup>4</sup> to account for cosmic events, internal particle generation and South Atlantic Anomaly activation. Events from the High Energy X-ray Timing Experiment (HEXTE), also onboard the spacecraft, proved too scarce to be useful.

Throughout this paper we will employ the orbital ephemeris of Deeter et al. (1991):

$$T_{\text{orb}} = \text{MJD } 43\,804.51998(1) + 1.70016772(1)E_{\text{orb}} - 5.2(5) \times 10^{-11} E_{\text{orb}}^2 \quad (1)$$

where  $T_{\text{orb}}$  corresponds to superior conjunction of the compact star and  $E_{\text{orb}}$  is the orbital cycle number. Assuming the 35-d epoch is determined by:

$$T_{35} = \text{MJD } 50\,041.0 + 34.85 E_{35} \quad (2)$$

where  $T_{35}$  corresponds to X-ray turn-on of the main-high state and  $E_{35}$  is the cycle number

<sup>3</sup><http://xte.gsfc.nasa.gov>

<sup>4</sup><http://lheawww.gsfc.nasa.gov/~stark/pca/pcabackest.html>

(M. Kunz, private communication), the precession phases sampled are  $\phi_{35} = 0.16\text{--}0.29$ . These would normally correspond approximately to the second half of a main-high state (Scott and Leahy 1999), but the average count rate of 4 counts  $\text{s}^{-1} \text{PCU}^{-1}$  testifies to the anomalous extended low-state in which Her X-1 had remained for the previous four 35-d cycles (Coburn et al. 2000). Count rates are of order 1 percent of the normal main-high state (dal Fiume et al. 1998).

### 3. Light curve

Standard2 data from each visit were filtered to reject pointings closer than 10 degrees to the Earth’s limb and those off-axis by 0.02 degrees or greater. From all PCA layers and columns, events were summed across pulse-height channels to provide a light curve in the energy range 3–30 keV with 1-ksec sampling. This is presented in Fig 1 and hardness ratios between 2–5 keV, 5–8 keV and 8–20 keV are provided in Fig 2 (eclipse data have been removed from the hardness diagrams). Background models have been subtracted and data di-

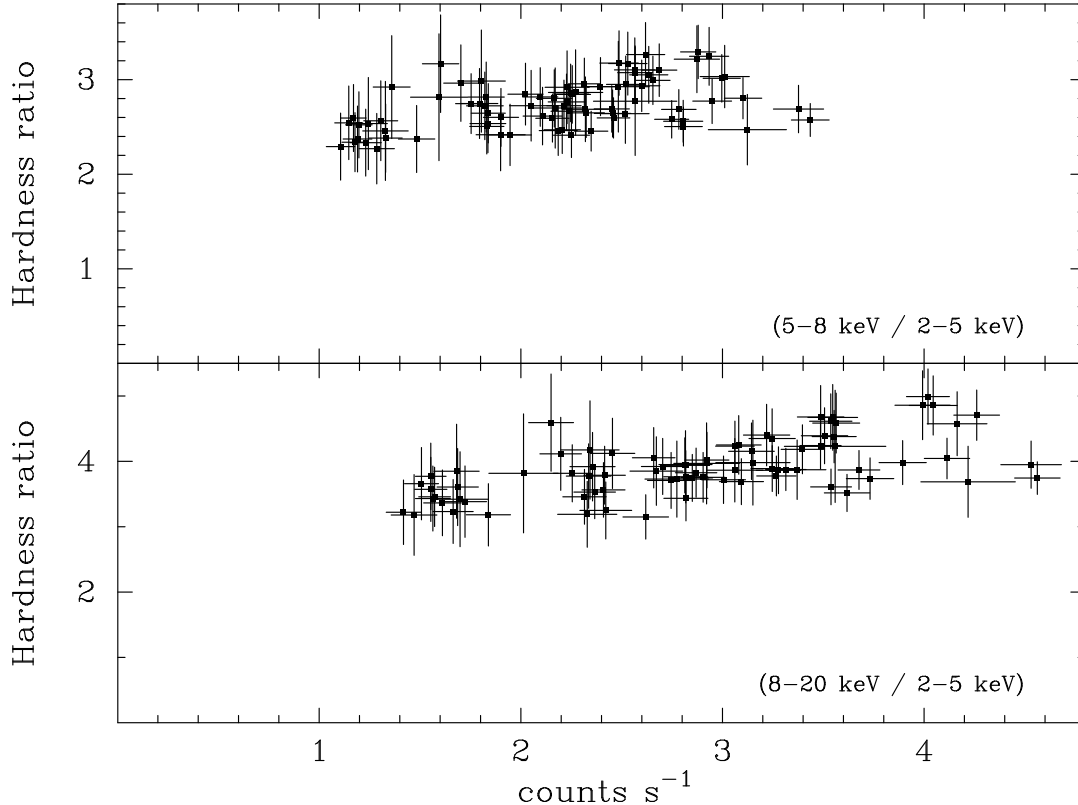


Fig. 2.— Hardness ratios for the bands 2–5 keV, 5–8 keV and 8–20 keV. Eclipse points,  $\phi_{\text{orb}} = -0.1$ – $0.1$ , have been excluded.

vided by the number of active PCUs.

Gerend & Boynton (1976) show that the majority of power from companion star emission occurs on the 1.7-d orbital frequency through stellar rotation. However, light curve structure associated with the accretion flow from the companion star, such as the hot spot and splash from the collision of stream and disk (Schandl 1996), occur on a timescale close to the beat period. Fig 1 shows an intensity modulation approximating the 1.7-d orbital period. Depending on its source, we expect the observed modulation to occur either on the orbital or 1.62-d beat period.

The hardness ratios of Fig. 2 indicate that the modulation is not the result of photo-electric absorption. We are observing intrinsic flux increases or opaque obstruction of a soft emission region. The observed structure occurs over timescales several factors longer than normal main-high dipping events (Leahy 1997).

Maximum flux corresponds approximately with orbital phase  $\phi_{\text{orb}} = 0.5$ , where  $\phi_{\text{orb}} = 0.0$  is superior conjunction of the neutron star. This is

consistent with a region associated with the irradiated inner surface of the companion star. The similarities between this light curve and the optical, UV and EUV light curves which are dominated by companion star emission are striking (Still et al. 1997; Leahy & Marshall 1999; Boroson et al. 2000). We suggest that the modulation is the result of Compton reflection of X-rays off the atmosphere of the companion, which was predicted by Basko, Sunyaev & Titarchuk (1974) and detected at EUV wavelengths by Leahy & Marshall (1999) and Leahy et al. (2000).

If we are detecting companion star reflection, there must be a second source of X-ray flux associated with the compact object in order to produce the narrow eclipses at MJD 51 372.0, MJD 51 373.7 and MJD 51 375.4. There are equivalent eclipses at optical and UV wavelengths which are thought to be the eclipse of disk light by the companion star (Gerend & Boynton 1976; Boroson et al. 2000).

After removing eclipses and using the Lomb-Scargle statistic (Scargle 1982), the best fit period to this light curve is  $1.74 \pm 0.06$ -d, with a false

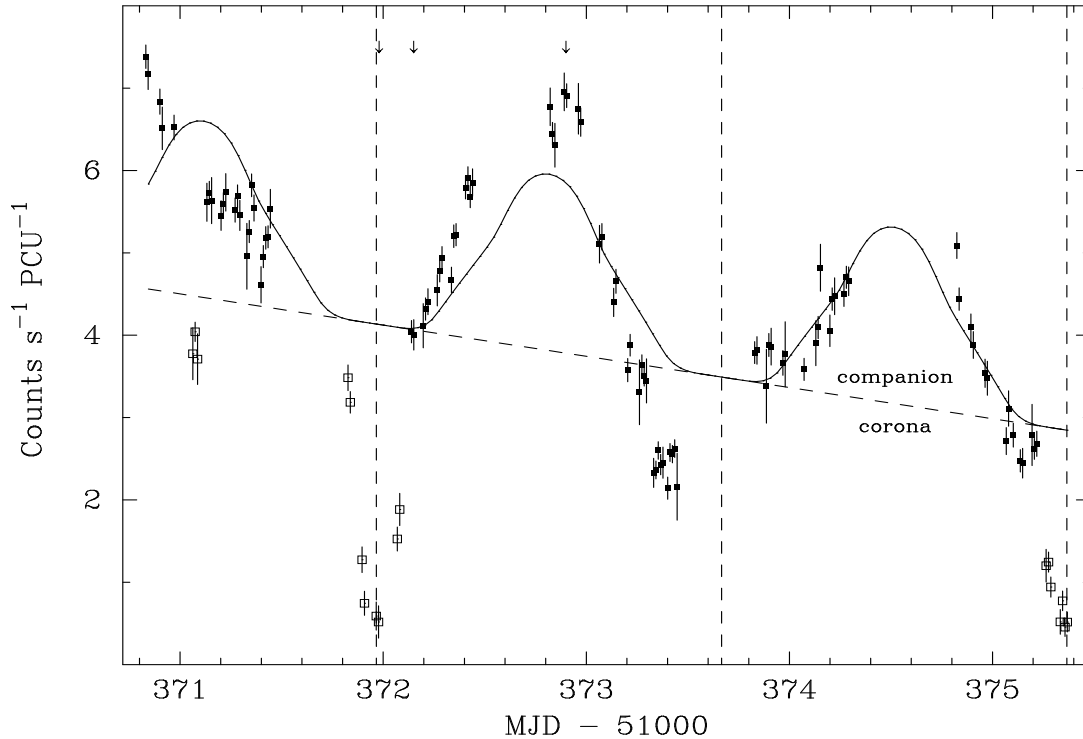


Fig. 3.— A fit to the light curve using the geometric binary synthesis code of Still et al. (1997) plus a linear-decay function to represent the corona. Points designated by open squares, corresponding to eclipses and the dip at MJD 51,371.05 were ignored by the fit. The dashed line is the coronal fit alone. The three spectra presented in Fig. 4 were extracted from the visits indicated by arrows.

alarm-probability of  $10^{-12}$ . The error is the  $\sigma$ -width of the peak in the power spectrum and can only discriminate between the orbital and beat frequencies to  $1.3\sigma$ .

We attempt a crude fit to the light curve where the reflection component is constructed by combining the geometric stellar synthesis code of Still et al. (1997) with the classical H-function reflection coefficients (Chandrasekhar 1960). Reflected flux between 3 and 30 keV is integrated over the stellar surface area. This is detailed in Appendix A. We adopt an orbital inclination of  $i = 82^\circ$ , a neutron star mass of  $M_{\text{ns}} = 1.4 M_\odot$  and a Roche lobe-filling companion star mass of  $M_{\text{com}} = 2.2 M_\odot$  (Reynolds et al. 1997). Unlike Still et al. (1997), and in order to reduce the number of free parameters, we do not attempt to model the shadow of the accretion disk over the companion star, or the orbital eclipse of the star by the disk, centered at  $\phi_{\text{orb}} = 0.5$ . The energy spectrum of the compact source is taken to be a powerlaw of slope  $\alpha = 0.9$  with an exponential cutoff at  $E_{\text{cut}} = 11$  keV (see Sec. 4). The luminosity of the

source is arbitrary, where the resulting reflection spectrum is rescaled such that the maximum count rate at  $\phi_{\text{orb}} = 0.5$  is  $1 \text{ count s}^{-1} \text{ PCU}^{-1}$ . The coronal component is represented by a linear function which is better statistically than a constant, such that the overall fit is given by:

$$L(t) = p_1 + p_2 t + p_3 R(t) \quad (3)$$

$p_1$  and  $p_2$  are the constant and linear terms of the coronal component, and  $p_3$  is a renormalization constant for the modeled companion star light curve  $R(t)$ .  $t$  is time in days after MJD 51,000.

After rejecting eclipse points and the dip at MJD 51 371.05, the fit was made using a Downhill Simplex Algorithm (Press et al. 1992). The result is plotted in Fig. 3 where  $p_1 = 145$ ,  $p_2 = -0.38$  and  $p_3 = 2.14$ ;  $\chi^2 = 2100$  for 84 dof. Decreasing coronal flux is consistent with the behaviour of direct photons from the accretion region during this phase of the normal 35-d cycle (Scott & Leahy 1999).

The fit is poor, although this is not particularly discouraging given our first-order treatment

of coronal variability. Residuals are probably dominated by the coronal component. In the following sections we perform spectral fits in an attempt to separate the two components, test the suitability of reflection for fitting the energy spectrum of the modulated component, and subtract modeled stellar reflection spectra to reveal the spectral variability of the corona.

#### 4. Energy spectrum

Under the same filtering constraints as above, the GoodXenon events were sampled with the full pulse-height resolution of the PCA. Channels 1–7 (< 3 keV) were ignored due to uncertain background modeling, and channels 63–256 (> 30 keV) ignored as a result of poor counting statistics. XSPEC v11 was used at all times. Spectral fits to three of the visits are presented in Fig 4.

##### 4.1. Corona spectrum

We consider a model where emission originates from two distinct binary regions, an accretion disk corona and the companion star. We first consider the corona, whose output is presumably the result of upscattering soft disk photons in a relatively hot medium (e.g. Sunyaev and Titarchuk 1980). For now, the parameters of this model will be considered constant over time (excluding eclipses), except for the normalization parameter which we will vary according to the linear component of our light curve fit from Sec. 3. This rather false constraint will allow us to separate approximately the two spectral components and is probably valid across neighboring visits, but not over a number of orbital cycles (Fig. 3).

The visit at MJD 51372.15 is the most likely to isolate the coronal component. Eclipse egress is approximately complete and any contribution from the reflection component is assumed negligible. We refrain from using the pre-eclipse visits at MJD 51 373.4 and MJD 51 375.2 in case dipping is occurring. An absorbed power law model of the form:

$$S(E) = \exp[-N_{\text{H}}\sigma(E)]AE^{-\alpha} \quad (4)$$

where  $A$  is the normalization,  $\sigma(E)$  the photoelectric cross-section (Balucinska-Church and McCammon 1992) and  $N_{\text{H}}$  the neutral hydrogen column density, provides an inadequate fit of  $\chi^2_{\text{red}} =$

2.06 for 54 dof. The addition of a Gaussian model:

$$G(E) = \frac{A_{\text{K}}}{\sqrt{2\pi\sigma_{\text{K}}^2}} \exp\left[-\frac{1}{2}\left(\frac{E - E_{\text{K}}}{\sigma_{\text{K}}}\right)^2\right] \quad (5)$$

representing an iron emission complex at 6.4–6.7 keV improves the fit to  $\chi^2_{\text{red}} = 1.15$  for 51 dof.  $A_{\text{K}}$  is the line flux,  $\sigma_{\text{K}}$  the line width and  $E_{\text{K}}$  the line center. Compared to previous observations of Her X-1 in anomalous low-states (e.g. Parmar et al. 1999; Coburn et al. 2000), the powerlaw component is rather steep,  $\alpha = 1.8 \pm 0.1$ , and the Fe line nested at high energy  $6.9 \pm 0.2$  keV. By introducing further complexity into the model both the powerlaw slope and line energy agree with previous results but the  $\chi^2$ -statistic cannot discriminate between a number of models. A definitive model is not essential since these fit parameters will remain fixed in order to extract approximately the reflection spectrum a few visits later. Therefore we choose a model which is simple but physically realistic, and is also compatible with fits made earlier in the anomalous low state by Coburn et al. (2000) – in this case a powerlaw with high-energy exponential cutoff, a Fe emission line and a partial-covering, cold absorber:

$$S(E) = P(E) \left[ A \exp\left(-\frac{E}{E_{\text{cut}}}\right) E^{-\alpha} + G(E) \right] \quad (6)$$

where

$$P(E) = (1 - f) + f \exp[-N_{\text{H}}\sigma(E)] \quad (7)$$

$f$  is the partial covering fraction and  $E_{\text{cut}}$  the cut-off energy. The excessive number of free parameters mean that the column density, covering fraction and powerlaw slope are poorly constrained. Since the current anomalous low-state is thought to be the result of obscuration rather than intrinsic source behaviour we can assume that the coronal photons have undergone elastic scattering and rationalize fixing the powerlaw slope to its main-high state value,  $\alpha = 0.9$  (Dal Fiume et al. 1998). From the visit at MJD 51 372.15,  $N_{\text{H}} = (1.6 \pm 0.8) \times 10^{23} \text{ cm}^{-2}$ ,  $f = 0.7 \pm 0.1$ ,  $E_{\text{cut}} = 11 \pm 2 \text{ keV}$ ,  $A = (2.6 \pm 0.9) \times 10^{-3} \text{ photons cm}^{-2} \text{ s}^{-1} \text{ keV}^{-1}$  at 1 keV,  $E_{\text{K}} = 6.7 \pm 0.1 \text{ keV}$  and  $\sigma_{\text{K}} = 0.7 \pm 0.2 \text{ keV}$  with a line strength of  $(2 \pm 1) \times 10^{-4} \text{ photons cm}^{-2} \text{ s}^{-1}$ .  $\chi^2_{\text{red}} = 0.85$  for 50 dof and the equivalent width of the Fe complex is 775 eV.

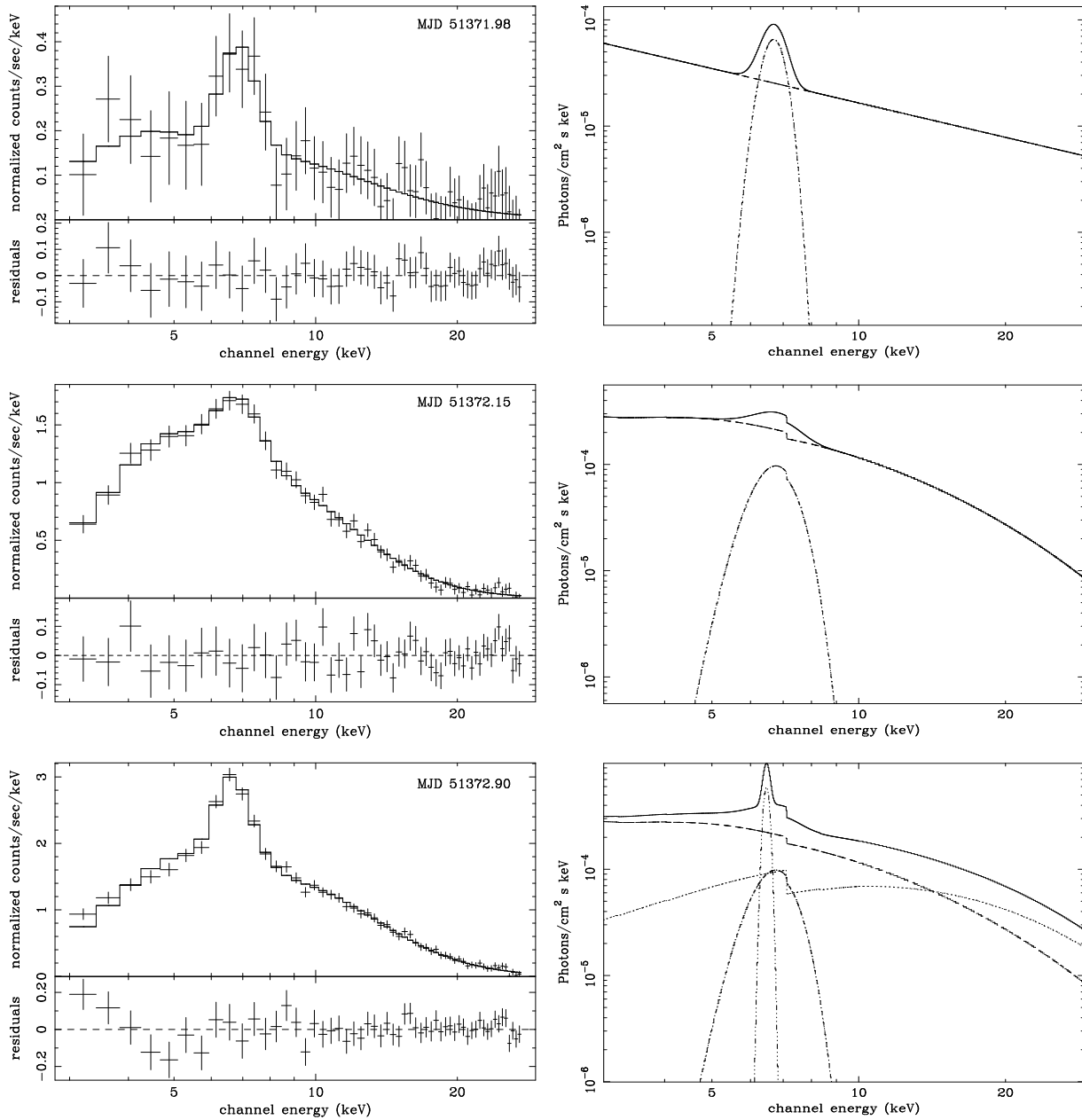


Fig. 4.— Spectral fits from three visits to Her X-1. The top left panel is a powerlaw + Gaussian profile fit to mid-eclipse data (MJD 51371.98). The right hand panel presents the best fit model. The middle two panels are the corresponding fit and model of the corona for the post-eclipse visit at MJD 51372.15 consisting of an exponentially-cutoff powerlaw and line, absorbed by a partial cover. The lower panels represent the visit at maximum flux, MJD 51372.90, where a reflection component and second line are added. See Sec. 4 for details of the spectral models.

We apply this same model to a visit at  $\phi_{\text{orb}} = 0.5$  (MJD 51 372.90). Keeping  $\alpha$  and  $E_{\text{cut}}$  fixed at their previous values provides a poor fit,  $\chi_{\text{red}}^2 = 2.74$  for 51 dof. Relaxing both these constraints yields an acceptable fit of  $\chi_{\text{red}}^2 = 0.74$  for 49 dof. However  $N_{\text{H}} = 0$  and  $\alpha$  is extremely flat,  $0.13 \pm 0.12$ . Consequently, in a time-variable capacity the coronal model alone does not fit the data sensibly. Therefore a two-source model is more appropriate.

## 4.2. Reflection spectrum

We would like to test whether reflection provides a good fit to the modulated component. Reflection would be the result of scattering of hard radiation from the accreting source off the relatively cold atmospheres of the companion star or accretion disk. The spectrum will suffer photoelectric absorption at energies less than 10 keV, have a strong Fe  $K\alpha$  line and will be down-scattered at energies higher than 50 keV. Thus, the reflection spectrum has a maximum in the *RXTE* PCA band at energies 15 – 20 keV.

As explained in the previous section, we assume the coronal model parameters are time-invariant, except for the normalization which is scaled by the light curve fit of Eqn. 3. This is in order to reduce the number of free parameters which is excessive for the quality of spectra from individual visits.

The visit we consider is at  $\phi_{\text{orb}} \simeq 0.5$  (MJD 51 372.90) which has a number of advantages over other observations. This phase provides the best counting statistics. Furthermore we expect to be observing  $\sim 100$  percent of the irradiated surface at this time so we can assume that all reflected flux is recorded. Finally we are reasonably close to the visit where the coronal spectrum was characterized and so our assumptions concerning the form and brightness of this component are hopefully valid. We test these assumptions in Sec. 6.

We first attempt adding a few simple models to the coronal component in an attempt to produce a statistically-acceptable fit. A second Gaussian component is always required. Adopting  $S(E) + \text{powerlaw} + \text{Gaussian}$  provides a  $\chi_{\text{red}}^2 = 1.17$  for 52 dof. The photon index is flat,  $\alpha = 0.33 \pm 0.1$ , and the fit yields a notable low-energy excess. A  $S(E) + \text{blackbody} + \text{Gaussian}$  yields  $\chi_{\text{red}}^2 = 0.72$  for 52 dof. The blackbody temperature is  $6.2 \pm 0.7$  keV

and the  $6.4 \pm 0.1$  keV line has an equivalent width of 3.13 keV. Despite the good fit, it is not obvious what would radiate thermally at this temperature within the framework of the anomalous low-state model (Vrtilek et al. 2001), or produce such a broad line. The low-energy excess remains a feature.

More realistically, we fit  $S(E) + \text{Gaussian} + \text{the elastic, cold Compton reflection model HREFL}$ . Although the geometry of this model is more suited to disk reflection than a Roche surface, it is the most-appropriate model within the XSPEC package and yields an approximate fit. This provides confidence in a more sophisticated approach undertaken in Sec. 6.

The fraction,  $f_{\text{esc}}$ , of direct X-rays observed is zero, since the point source is obscured by the accretion disk. However much of the companion star atmosphere has a largely-unobscured view of the X-ray source. The reflection model assumes an isotropically-radiating point source of a given energy spectrum and flux that irradiates a structure subtending a solid angle  $\omega$  on the sky with respect to the point source. By adopting stellar masses of  $M_{\text{ns}} = 1.4 M_{\odot}$  and  $M_{\text{com}} = 2.2 M_{\odot}$ , and companion radial velocity of  $100 \text{ km s}^{-1}$  (Reynolds et al. 1997), we find  $\omega = 0.15\pi$ . We approximate a reflecting structure incident to X-rays at all angles between  $\theta_{\text{min}} = 0$  degrees and  $\theta_{\text{max}} = 90$  deg, weighted equally, and inclined on the sky at an angle  $\theta_{\text{obs}} = 0$  deg to the observer at  $\phi_{\text{orb}} = 0.5$  and orbital inclination  $i \simeq 90$  degrees. Solar abundances were adopted. The incident energy spectrum is modeled by the same cut-off powerlaw as before with  $\alpha = 0.9$  and  $E_{\text{cut}} = 11$  keV.

The photon flux of the irradiating powerlaw spectrum and Gaussian profile provide just four free parameters, yielding a  $\chi_{\text{red}}^2$  of 0.89 for 53 dof. Fit parameters are listed in Tab. 1. The fit is extremely good considering there is only one free parameter available to define the reflection continuum. Encouragingly, photon flux for the unseen powerlaw source at 1 keV is  $(9.0 \pm 0.9) \times 10^{-2}$  photons  $\text{cm}^{-2} \text{ s}^{-1} \text{ keV}^{-1}$ . The flux from a typical main-high state of Her X-1 is 0.1 photons  $\text{cm}^{-2} \text{ s}^{-1} \text{ keV}^{-1}$  at 1 keV (dal Fiume et al. 1998). The line is strong, narrow and nested at low Fe  $K\alpha$  energies, as predicted by reflection models (Basko et al. 1974; Ross & Fabian 1993). This consistency, combined with the period and phasing of



the modulated component all point to the companion star providing the reflective surface.

### 4.3. Eclipse spectrum

The visit during mid-eclipse (MJD 51371.98) is fit well with a single powerlaw,  $\chi_{\text{red}}^2 = 0.93$  for 26 dof over channels 8–35 (3–15 keV). Although the inclusion of a Fe line is not formally required, there is an excess longward of the Fe K edge. Including a Gaussian model suggests a line of equivalent width 2.6 keV, where  $\chi_{\text{red}}^2 = 0.39$  for 23 dof. Here  $\alpha = 1.2 \pm 0.3$ ,  $A = (2 \pm 1) \times 10^{-4}$  photons  $\text{keV}^{-1} \text{cm}^{-2} \text{s}^{-1}$  at 1 keV,  $E_{\text{K}} = 6.7 \pm 0.3$  keV and  $\sigma_{\text{K}} = 0.3 \pm 0.2$  keV with a line intensity of  $(6 \pm 3) \times 10^{-5}$  photons  $\text{cm}^{-2} \text{s}^{-1}$ . Adopting a cut-off powerlaw model of  $\alpha = 0.9$  and  $E_{\text{cut}} = 11$  keV and fitting just the normalization and line parameters yields consistent Gaussian characteristics within the uncertainties.

### 5. Pulse timing

In this section we report the detection of spin pulses, measure their frequency and present pulse profiles. GoodXenon data were extracted over all energy channels and binned to 0.02-s. Times were corrected to the compact sources local standard of rest using the orbital time-delay semi-amplitude determined by Deeter et al. (1991) and the spin period of the pulsar was searched for using the Lomb-Scargle algorithm. A period of  $1.237746 \pm 0.000001$ -s was found with a false-alarm probability of  $10^{-5}$ . This is consistent with the measurements of Parmar et al. (1999) and Coburn et al. (2000) during the same anomalous low-state and signifies that the pulsar has spun down during the low-state episode, as it has in the previous two recorded anomalous low epochs (Vrtilek et al. 1994). Coburn et al. (2000) discuss the implications of these spin-down episodes with regard to the accretion torque in the system. The pulse profile is presented in Fig. 5.

It is unlikely that the observed pulses are within reflected light from the companion star. The spin frequency is constant in the rest-frame of the compact object so should be scattering off the accretion disk or accretion disk corona. Pulse fractions are of the order a few percent whereas models of reflected pulses off the companion predict fractions an order of magnitude less (Middleditch and Nel-

son 1976).

### 6. Modeling Roche lobe reflection

The current family of reflection models available in XSPEC v11 are not well-suited to our problem. These were developed for accretion disk reflection problems (see e.g. Magdziarz & Zdziarski 1995) and limit our results because of incorrect geometry. The models available assume the reflecting body is a uniform slab, viewed at an inclination angle and illuminated by a point source above the surface of the slab. The size of the slab and the distance from the point source are characterized by a filling factor – the fraction of sky occupied by the slab with respect to the source. The model adopted in Sec. 4.2 takes into account a range of equally-weighted irradiance angles to approximate the curved Roche surface of the star, but it is again a simplification of the problem (although a valuable consistency check for more sophisticated models). The simplified model did indicate however that the reflected flux was identical (within the  $1\text{-}\sigma$  measurement uncertainty) to that expected from a point source with the distance, energy spectrum, and intensity of Her X-1 at the peak of its main-high state. We would like to test this more rigorously by defining an accurate reflection surface.

In order to treat the problem more accurately we develop a code which divides the surface of a Roche lobe-filling star into small, discrete elements. Each has an individual inclination angle with respect to the Earth. Each has an individual grazing incidence angle and filling factor with respect to the X-ray source. Our task is to determine these parameters over a grid using Roche geometry and sum the reflection spectrum over all observer-visible surface elements. This approach both treats the geometry correctly and allows a fit to be made at any orbital phase. Again, we follow the algorithm described in Appendix A.

The model was developed as an external, multiplicative XSPEC package and applied to the spectrum sampled at MJD 51372.90 where we fit the composite model of Eqn. 6, by replacing the HREFL component and adopting the fixed coronal and pulsar parameters listed in Tab. 1. Our reflection parameters are stellar mass ratio  $q = M_{\text{com}}/M_{\text{ns}}$ , which defines the shape of the companion star

TABLE 1

BEST-FIT PARAMETERS FOR THE THREE SPECTRA PRESENTED IN FIG. 4. ALL FITS ARE ALSO SUBJECT TO A FIXED INTERSTELLAR COLUMN DENSITY OF  $5.1 \times 10^{19} \text{ cm}^{-2}$  (DAL FIUME 1998). THE REFLECTION PARAMETERS ARE GIVEN FOR MJD 51 372.90.

Eclipse parameters	
$\alpha$	$1.2 \pm 0.4$
$A$ (ph $\text{cm}^{-2} \text{ s}^{-1} \text{ keV}^{-1}$ )	$(2 \pm 1) \times 10^{-4}$
$E_{\text{K}}$ (keV)	$6.7 \pm 0.3$
$\sigma_{\text{K}}$ (keV)	$0.3 \pm 0.2$
$A_{\text{K}}$ (ph $\text{cm}^{-2} \text{ s}^{-1}$ )	$(6 \pm 3) \times 10^{-5}$
Coronal parameters	
$N_{\text{H}}$ ( $\times 10^{22} \text{ cm}^{-2}$ )	$16 \pm 12$
$f$	$0.7 \pm 0.6$
$\alpha^{\text{a}}$	0.9
$E_{\text{cut}}$ (keV)	$11 \pm 2$
$A$ (ph $\text{cm}^{-2} \text{ s}^{-1} \text{ keV}^{-1}$ )	$(3 \pm 1) \times 10^{-3}$
$E_{\text{K}}$ (keV)	$6.7 \pm 0.2$
$\sigma_{\text{K}}$ (keV)	$0.7 \pm 0.4$
$A_{\text{K}}$ (ph $\text{cm}^{-2} \text{ s}^{-1}$ )	$(2 \pm 1) \times 10^{-4}$
Reflection parameters	
$\alpha^{\text{a,b}}$	0.9
$E_{\text{cut}}$ (keV) <sup>a,b</sup>	11
$A$ (ph $\text{cm}^{-2} \text{ s}^{-1} \text{ keV}^{-1}$ ) <sup>b</sup>	$(9.0 \pm 0.9) \times 10^{-2}$
$\omega^{\text{a}}$	$0.15\pi$
$\cos \theta_{\text{obs}}^{\text{a}}$	1
$\cos \theta_{\text{min}}^{\text{a}}$	1
$\cos \theta_{\text{max}}^{\text{a}}$	0
Fe abundance (solar) <sup>a</sup>	1
$f_{\text{esc}}^{\text{a}}$	0
$E_{\text{K}}$ (keV)	$6.5 \pm 0.1$
$\sigma_{\text{K}}$ (keV)	$0.1 \pm 0.1$
$A_{\text{K}}$ (ph $\text{cm}^{-2} \text{ s}^{-1}$ )	$(1.5 \pm 0.2) \times 10^{-4}$

<sup>a</sup>Frozen parameter.

<sup>b</sup>Model component is directly-invisible to the observer.

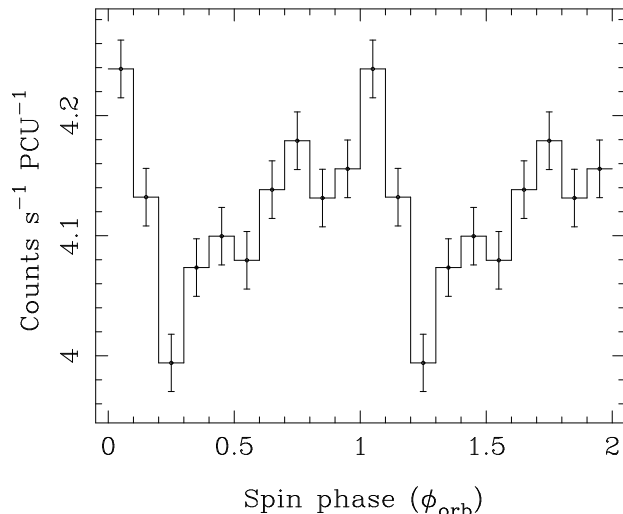


Fig. 5.— Time-averaged spin pulse from Her X-1. The pulse cycle is repeated for clarity.

and the area of pulsar-sky each surface element occupies, the orbital inclination,  $i$ , and the orbital phase,  $\phi_{\text{orb}}$ , which together define those elements of the stellar surface visible to Earth. We use the spectroscopic measurements of Reynolds et al. (1997),  $q = 1.57$  and  $i = 82^\circ$ . The orbital ephemeris of Eqn. 1 indicates  $\phi_{\text{orb}} = 0.55$ . In order to calculate the scattering probability the Fe abundance is adopted as solar.

As before, four free parameters remain, yielding a reduced  $\chi^2$  of 0.86 for 53 dof, where  $A = (9.6 \pm 0.5) \times 10^{-2}$  photons  $\text{s}^{-1} \text{cm}^{-2} \text{keV}^{-1}$  at 1 keV,  $E_K = 6.5 \pm 0.1$  keV,  $\sigma_K = 0.1 \pm 0.1$  keV and  $A_K = (1.4 \pm 0.2) \times 10^{-4}$  photons  $\text{s}^{-1} \text{cm}^{-2}$ . This is both consistent with the HREFL model and confirms that the intrinsic flux from the pulsar is reproduced with reflection off a Roche surface at this orbital phase.

At  $\phi_{\text{orb}} = 0.5$  the Roche reflection model most-resembles the disk reflection models. Ideally we would like to apply the test above to all orbital phases but Fig. 3 indicates that if stellar reflection drives the orbital light curve, then the coronal spectrum is variable and our model assumptions break down. The alternative approach is to freeze  $A$ , calculate the reflection spectrum at each visit and then fit the coronal model to the residuals.

Since it is not possible to separate the coronal and reflected Fe lines, these are fit with just a single Gaussian. Neglecting the short-term behaviour of the absorbing column and coronal line flux, we expect Gaussian strength,  $A_K$ , and width,  $\sigma_K$ , to vary with the reflection continuum as a result of the narrow fluorescence line from the companion

star varying over the orbital cycle. The 3–30 keV reflection flux (top panel) and the best fit parameters for all visits are presented in Fig. 6. Both the coronal  $\alpha$  and  $E_{\text{cut}}$  were frozen during the fits.

Coronal parameters are expected to vary on the 35-d, rather than the 1.7-d cycle and we see no detectable orbital coherency in  $N_{\text{H}}$ ,  $f$  or  $A$ . The decay of the coronal flux appears related to a long-term increase in  $N_{\text{H}}$ , rather than a decrease in  $A$ , which is consistent with the 35-d disk precession model for Her X-1 (c.f. Scott & Leahy 1999). As predicted,  $A_K$  is modulated on the orbital period, with a maximum at  $\phi_{\text{orb}} \simeq 0.5$ , although similar coherency is not discernible in  $\sigma_K$ .

## 7. Discussion

Despite the reflection effect in Her X-1 being observed in the EUV band (Leahy & Marshall 1999; Leahy et al. 2000), this is the first convincing detection of the phenomenon at X-ray energies. Basko et al. (1974) demonstrated that X-ray reflected flux from the companion star in Her X-1 should be at the level a few percent of the intrinsic radiation. This should generally be washed out by shot noise from the central source during normal main-high states, but as in the current observations, should also be observable during normal low states of the 35-d cycle. Sheffer et al. (1992) claimed a tentative detection of reflection during a normal off-state during the *ASTRON* mission, but a systematic search for this effect during normal or anomalous low-states has never been undertaken; the HEASARC archive is not rich with data from these epochs and those that exist coincide with

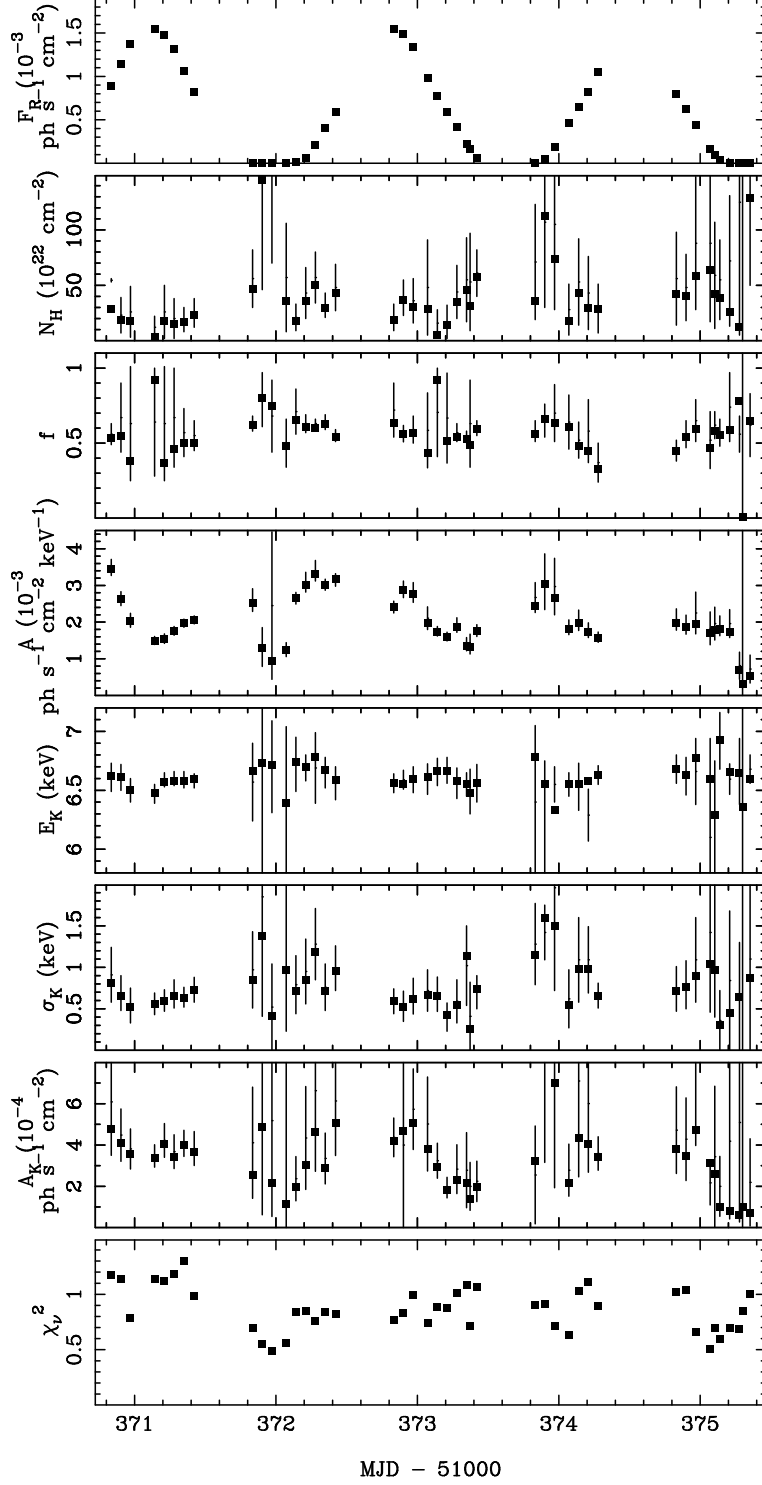


Fig. 6.— The top panel presents the predicted 3–30 keV reflected flux from the companion star as a function of MJD. The remaining panels illustrate the fit parameters of the coronal continuum model and a single Gaussian fitting both coronal and reflected Fe components after the reflection continuum has been subtracted. The bottom panel provides the reduced  $\chi^2$  for each fit.

eclipses of the pulsar (e.g. Choi et al. 1997). Exceptions are the *EXOSAT* pointings by Parmar et al. (1985), the *BeppoSAX* observations of Parmar et al. (1999) and the *RXTE* visits by Coburn et al. (2000). None of these analyses consider reflection as a possible interpretation of data, but the count rates presented by Parmar et al. (1985; 1999) arguably both display 1.7-d modulation. The baseline of the Coburn et al. (2000) visits is 20 ksec covering  $\phi_{\text{orb}} = 0.64\text{--}0.77$ . The general trend in count rate over this period is one of decline, as predicted by the reflection model (Fig. 3), although the count rate and decline are a factor two larger than the current data.

Potentially, Her X-1 contains a rich lode of reflection physics. The reflection effect is common to a large number of different X-ray sources such as AGN and stellar mass black hole (Lightman & White; White et al. 1988). But generally there is uncertainty concerning the physical location and size of hard radiation sources in these objects, and the size and shape of the reflecting atmosphere (which in these cases is presumably an accretion disk). Therefore Her X-1 is an ideal X-ray source for studying the properties of reflection and associated processes (such as winds and coronae etc) because we have a relatively clear picture of companion star geometry and its illumination by well-measured hard radiation from a central object.

Despite this there are some limitations. Firstly it is not clear how, or whether, the X-ray emission from the pulsar is beamed, or how column density changes with disk inclination angle. Although the high inclination of the binary means the observer has a similar line of sight to the source as the equatorial regions of the companion star, surface elements closer to the stellar poles may perceive the central source differently. In this paper we have assumed the source is an isotropic emitter. Also we assume that the X-ray source is point-like. This is not true, since we observe scattered light from a disk corona and expect further scattering and reflection from the disk itself; Leahy (1995) showed that soft photons come from an extended region using eclipse timings. Furthermore we made no attempt to model the accretion disk shadow, or its eclipse, over the equatorial regions of the companion star since the disk shape is so poorly constrained. The reflection process itself is also treated simply. More sophisticated models by

(e.g. Ross & Fabian 1993; Nayakshin 2000) consider the physical response of an atmosphere to irradiation and the resultant spectral changes.

There is scope for much more observation. The reflection model can be tested more sensitively with improved models and greater energy resolution using grating spectrometers sensitive to soft energies below 1 keV which should be populated by resonance absorption edges (Basko et al. 1974), and over the Fe  $\alpha$  complex to resolve and separate line components between corona and companion star. In order to constrain the location of reflection, timing experiments with improved sampling over the 35-d cycle would determine whether light curve modulation is driven on the orbital (1.7-d) or beat (1.6-d) period. Fast timing visits during eclipses of the companion by the accretion disk at  $\phi_{\text{orb}} = 0.5$  can help constrain the shape of the accretion disk using the eclipse ingress and egress profiles.

## 8. Conclusion

Over 2.7 orbital cycles during the anomalous low-state of 1999 the X-ray pulsar Her X-1 displayed an X-ray light curve very similar to optical and UV counterparts, suggesting that the companion star contributes to X-ray emission. A cold Compton reflection spectrum was successfully fit to the variable component of the energy spectrum. By employing binary geometry and assuming companion star reflection, the intensity of the hidden pulsar was found to be identical to the main-high state of the source when the pulsar is visible. This result indirectly implies the anomalous low-state model is correct – intrinsic accretion luminosity remains constant, but is occulted along the observers line-of-sight by the accretion disk.

This work was funded by NASA grant NRA-99-01-ADP-108, NAG5-6711 and NAG5-7333. KO, KH and HQ acknowledge support from the Particle Physics and Astronomy Research Council. This research has made use of data obtained from the High Energy Astrophysics Science Archive Research Center (HEASARC), provided by NASA’s Goddard Space Flight Center.

## REFERENCES

- Balucinska-Church M., McCammon D., 1992, *ApJ*, 400, 699
- Basko M. M., 1978, *ApJ*, 223, 268
- Basko M. M., Sunyaev R. A., Titarchuk L. G., 1974, *A&A*, 31, 249
- Boroson B., Kallman T., Vrtilik S. D., Raymond J., Still M., Bautista M., Quaintrell H., 2000, *ApJ*, 529, 414
- Boroson B., O'Brien K., Horne K., Kallman T., Still M., Boyd P., Quaintrell H., Vrtilik S. D., 2001, *ApJ*, 545, 399
- Coburn W., Heindl W. A., Wilms J., Gruber D. E., Staubert R., Rothschild R. E., Postnov K. A., Shakura N., Risse P., Kreykenbohm I., Pelling M. R., 2000, *ApJ*, 543, 351
- Chakrabarti S., Titarchuk L. G., 1995, *ApJ*, 455, 623
- Chandrasekhar S., 1960, *Radiative Transfer* (New York: Dover)
- Choi C. S., Seon K. I., Dotani T., Nagase F., 1997, *ApJ*, 476, 81L
- Dal Fiume D., Orlandini M., Cusumano G., Del Sordo S., Feroci M., Frontera F., Oosterbroek T., Palazzi E., Parmar A. N., Santangelo A. Segreto, A., 1998, *A&A*, 329, 41L
- Deeter J. E., Boynton P. E., Miyamoto S., Kitamoto S., Nagase F., Kawai N., 1991, *ApJ*, 383, 324
- Deeter J. E., Scott M. D., Boynton P. E., Miyamoto S., Kitamoto S., Takahama S., Nagase F., 1998, *ApJ*, 502, 802
- Gerend D., Boynton P. E., 1976, *ApJ*, 209, 562
- Giacconi R., Gursky H., Kellogg E., Levinson R., Schreier E., Tananbaum H., 1973, *ApJ*, 184, 227
- Leahy D. A., 1995, *ApJ*, 450, 339
- Leahy D. A., 1997, *MNRAS*, 287, 62
- Leahy D. A., Marshall H., 1999, *ApJ*, 521, 328
- Leahy, D. A., Marshall, H., Scott, D. M., 2000, *ApJ*, 542..446
- Lightman A. P., White T. R., 1988, *ApJ*, 335, 57L
- Magdziarz P., Zdziarski A. A., 1995, *MNRAS*, 273, 837
- Middleditch J., Nelson J. E., 1976, *ApJ*, 208, 567
- Morrison R., McCammon D., 1983, *ApJ*, 270, 119
- Nayakshin S., 2000, *ApJ*, 534, 718
- O'Brien K., Horne K., Hynes R. I., Chen W., Haswell C. A., Still M. D., 2000, *MNRAS*, submitted
- Papaloizou J. C. B., Terquem C., 1995, *MNRAS*, 274, 987
- Parmar A. N., White N. E., Barr P., Pietsch W., Truemper J., Voges W., McKechnie S., 1985, *Nature*, 313, 119
- Parmar A. N., Oosterbroek T., Del Sordo S., Segreto A., Santangelo A., Dal Fiume D., Orlandini M., 1999, *A&A*, 353, 575
- Press W. H., Teukolsky S. A., Vetterling W. T., Flannery, B. P., 1992, *Numerical Recipes: The Art of Scientific Computing*, 2nd edn, (CUP)
- Pringle J. E., 1996, *MNRAS*, 281, 357
- Reynolds A. P., Quaintrell H., Still M. D., Roche P., Chakrabarty D., Levine S. E., 1997, *MNRAS*, 288, 43
- Ross R. R., Fabian A. C., 1993, *MNRAS*, 261, 74
- Rutten R. G. M., Dhillon V. S., 1994, *A&A*, 288, 773
- Scargle J. D., 1982, *ApJ*, 263, 835
- Schandl S., 1996, *A&A*, 307, 95
- Scott D. M., Leahy D. A., 1999, *ApJ*, 510, 974
- Sheffer E. K., Kopaeva I. F., Averintsev M. B., Bisnovaty-Kogan G. S., Golynskaya I. M., Gurin L. S., Dyachkov A. V., Zenchenko V. M., Kurt V. G., Mizyakina T. A., Mironova E. N., Sklyankin V. A., Smirnov A. S., Titarchuk L. G., Shamolin V. M., Shafer E. Y., Shmelkin A. A., Giovannelli F., 1992, *SvA*, 36, 41

- Still M. D., Quaintrell H., Roche P., Reynolds A. P., 1997, MNRAS, 292, 52
- Still M., O'Brien K., Horne K., Hudson D., Boroson B., Vrtilek S. D., Quaintrell H., Fiedler H., 2001, ApJ, submitted
- Sunyaev R. A., Titarchuk L. G., 1980, A&A, 86, 121
- Tananbaum H., Gursky H., Kellogg E. M., Levinson R., Schreier E., Giacconi R., 1972, ApJ, 174, L143
- Vrtilek S. D., Mihara T., Primini F. A., Kahabka P., Marshall H., Agerer F., Charles P. A., Cheng F. H., Dennerl K., La Dous C., Hu E. M., Rutten R., Serlemitsos P., Soong Y., Stull J., Truemper J., Voges W., Wagner R. M., Wilson R., 1994, ApJ, 436, L9
- Vrtilek S. D., Quaintrell H., Boroson B., Still M. D., Fiedler H., O'Brien K., Raymond J. R., Kallman T., McCray R., 2001, 548, 471
- White T. R., Lightman A. P., Zdziarski A. A., 1988, ApJ, 331, 939
- Zhang W., Giles A. B., Jahoda K., Soong Y., Swank J. H., Morgan E. H., 1993, in EUV, X-ray and Gamma-ray Instrumentation for Astronomy iv, ed. O. H. Siegmund, (SPIE: Bellingham WA), p. 324

## A. Classical Compton reflection off a Roche lobe-filling surface

In order to estimate the stellar-reflected flux one must know the fraction of X-rays intercepted by the atmosphere of the companion and also the reflection properties of that atmosphere. The following calculations construct a stellar surface confined by the Roche equipotential surface of a binary of stellar mass ratio  $q = M_{\text{com}}/M_{\text{ns}}$  (Sec. A.1). They then determine the monochromatic Compton reflected fraction off discrete surface elements and sum the reflected flux in those elements visible to the observer at binary inclination  $i$  and binary phase  $\phi_{\text{orb}}$  (Sec. A.2).

### A.1. Roche geometry

The critical Roche potential is defined by:

$$\Psi_{\text{cr}} = \frac{q}{r_{\text{cr}}} + \frac{1}{1 - r_{\text{cr}}} + \frac{(1 + q)r_{\text{cr}}^2}{2} \quad (\text{A1})$$

$r_{\text{cr}}$  is normalized to the stellar separation and determined by minimizing  $|\epsilon_{\text{cr}}/(d\epsilon_{\text{cr}}/dr_{\text{cr}})|$ , where

$$\epsilon_{\text{cr}} = (1 + q)r_{\text{cr}} - 1 - \frac{q}{r_{\text{cr}}^2} + \frac{1}{(1 - r_{\text{cr}})^2} \quad (\text{A2})$$

Using a spherical polar coordinate system  $(r, \theta, \phi)$ , with an origin at the center of mass of the companion star, the stellar surface is divided over  $\theta$  and  $\phi$  into segments of equal solid angle (see Fig. 7). For any given  $\theta$  and  $\phi$ ,  $r$  is determined by minimizing  $|\epsilon/(d\epsilon/dr)|$ , where

$$\epsilon = \frac{q}{r} + (1 + r^2 - 2r \cos \theta)^{1/2} + \frac{(1 + q)r^2 \cos^2 \theta}{2} + \sin^2 \theta \cos^2 \phi + \frac{1}{2(1 + q)} - r \cos \theta - \Psi_{\text{cr}} \quad (\text{A3})$$

Following the approach previously adopted by Rutten and Dhillon (1994) and Still et al. (1997), each surface segment is divided into two, such that the critical Roche surface is completely tiled by  $N$  triangles. This provides a better approximation to a curved surface than other polygons. The coordinates of each triangle vertex,  $\mathbf{V}_{jk} = (r_{jk}, \theta_{jk}, \phi_{jk})$ , where  $j = 1$  to 3 and  $k = 1$  to  $N$ , are calculated using Eqns. A1–A3 and converted to a Cartesian coordinate system  $(x_{jk}, y_{jk}, z_{jk})$  with an origin at the center of mass using:

$$x_{jk} = r_{jk} \cos \theta_{jk} - \frac{1}{1 + q} \quad (\text{A4})$$

$$y_{jk} = r_{jk} \sin \theta_{jk} \cos \phi_{jk} \quad (\text{A5})$$

$$z_{jk} = r_{jk} \sin \theta_{jk} \sin \phi_{jk} \quad (\text{A6})$$

The coordinate center of each triangle is  $\mathbf{T}_k = \sum_{j=1}^3 (x_{jk}/3, y_{jk}/3, z_{jk}/3)$ . The unit vector normal of each triangular surface is

$$\mathbf{n}_k = \frac{(\mathbf{V}_{2k} - \mathbf{V}_{1k}) \times (\mathbf{V}_{3k} - \mathbf{V}_{1k})}{|(\mathbf{V}_{2k} - \mathbf{V}_{1k}) \times (\mathbf{V}_{3k} - \mathbf{V}_{1k})|} \quad (\text{A7})$$

where the surface area of each element  $A_k = |\mathbf{n}_k|/2$ . The cosine of a surface elements normal vector and the unit direction vector to Earth,  $\mathbf{e}$ , is the incidence angle of reflected photons:

$$\mu_k = \mathbf{n}_k \cdot \mathbf{e} \quad (\text{A8})$$

$\mathbf{e}$  is defined using the orbital inclination of the binary,  $i$ , and the orbital phase,  $\phi_{\text{orb}}$ .

$$e_x = \sin i \cos(\pi(1 - 2\phi_{\text{orb}})) \quad (\text{A9})$$

$$e_y = \sin i \sin(\pi(1 - 2\phi_{\text{orb}})) \quad (\text{A10})$$



$$e_z = \cos i \quad (\text{A11})$$

Similarly the cosine of each elements normal vector with the unit vector direction to the X-ray source yields the incidence angle of photons arriving at the stellar surface:

$$\nu_k = n_k \cdot \frac{\mathbf{d}_k}{|\mathbf{d}_k|} \quad (\text{A12})$$

where

$$\mathbf{d}_{x,k} = -\mathbf{T}_{x,k} + \frac{q}{1+q} \quad (\text{A13})$$

$$\mathbf{d}_{y,k} = -\mathbf{T}_{y,k} \quad (\text{A14})$$

$$\mathbf{d}_{z,k} = -\mathbf{T}_{z,k} \quad (\text{A15})$$

and  $|d_k|$  is the distance between the source and each triangle. We assume the X-ray source is point-like and is coincident with the center of mass of the pulsar. Finally the solid angle of sky subtended by each triangle with respect to the X-ray source is

$$\omega_k = \nu_k \left[ 1 - \cos \left( \tan^{-1} \left( \frac{\sqrt{A_k/\pi}}{|d_k|} \right) \right) \right] \quad (\text{A16})$$

## A.2. Reflected flux

In Chakrabarti and Titarchuk (1995) the reflection problem in a plane geometry was solved exactly using the Fokker-Plank treatment for multiple scattered photons. Photoelectric absorption and downscattering effects were taken into account correctly. They suggest that in the very non-relativistic energy range,  $< 30$  keV the downscattering effects are negligible. Photons scatter off electrons almost coherently and consequently the results of the classical reflection problem are applicable (Chandrasekhar 1960). If the intrinsic flux spectrum from a point source radiating isotropically from the location of the pulsar is  $F_E$ , the reflected flux observed off all surface elements is

$$f_E = \frac{\lambda_E F_E}{2} \sum_{k=1}^N \frac{\omega_k \mu_k}{\mu_k + \nu_k} H(\lambda_E, \mu_k) H(\lambda_E, \nu_k) \quad (\mu_k > 0, \nu_k > 0) \quad (\text{A17})$$

Unobservable elements with  $\mu_k < 0$  and elements not incident to photons from the pulsar,  $\nu_k < 0$ , should be removed from the sum.  $\lambda_E$  is the photon scattering probability approximated by the piecewise polynomial fit of Morrison & McCammon (1983).  $H(\lambda_E, \beta)$  is the classical H-function (Chandrasekhar 1960), approximated with an uncertainty of  $< 1\%$  using the analytical expression of Basko (1978):

$$H(\lambda_E, \beta) = \frac{1 + \sqrt{3}\beta}{1 + \sqrt{3(1 - \lambda_E)\beta}} \left[ 1 - \frac{\lambda_E \beta}{4} (1 + \lambda_E^2) (\ln \beta + 1.33 - 1.458\beta^{0.62}) \right] \quad (\text{A18})$$

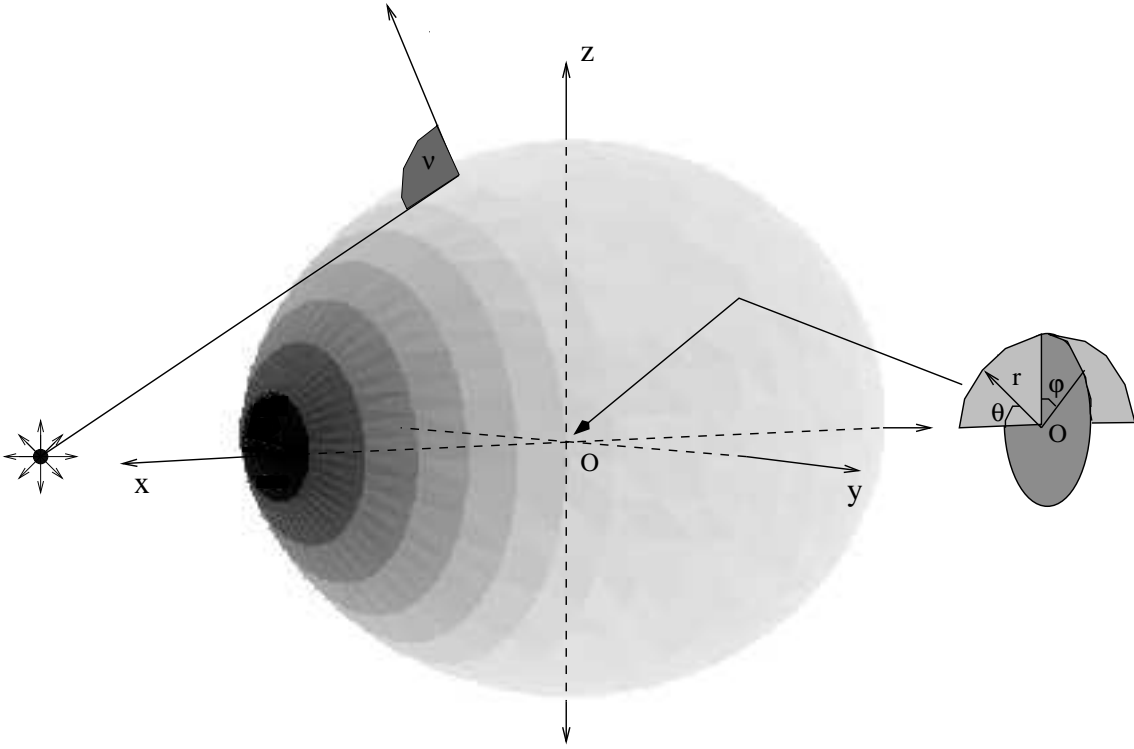


Fig. 7.— Schematic of the geometry used to determine the reflected spectrum, both cartesian and polar coordinates are displayed.  $\nu$  is the incidence angle of reflection relative to the neutron star. The incidence angle between surface elements and the observers line of sight,  $\mu$ , is the projection angle of each surface element on the page.